ELSEVIER

Transport mechanisms in nanopores and nanochannels: can we mimic nature?

Mario Tagliazucchi and Igal Szleifer*

Department of Biomedical Engineering, Department of Chemistry and Chemistry of Life Processes Institute, 2145 Sheridan Road, Northwestern University, Evanston, IL 60208, United States

The last few years have witnessed major advancements in the synthesis, modification, characterization and modeling of nanometer-size solid-state channels and pores. Future applications in sensing, energy conversion and purification technologies will critically rely on qualitative improvements in the control over the selectivity, directionality and responsiveness of these nanochannels and nanopores. It is not surprising, therefore, that researchers in the field seek inspiration in biological ion channels and ion pumps, paradigmatic examples of transport selectivity. This work reviews our current fundamental understanding of the mechanisms of transport of ions and larger cargoes through nanopores and nanochannels by examining recent experimental and theoretical work. It is argued that that structure and transport in biological channels and polyelectrolyte-modified synthetic nanopores are strongly coupled: the structure dictates transport and transport affects the structure. We compare synthetic and biological systems throughout this review to conclude that while they present interesting similarities, they also have striking differences.

Introduction

Living organism are structured in compartmentalized environments separated by membranes: inside a cell, organelles have membranes that separate them from the cytoplasm, cells have outer membranes that separate them from the extracellular matrix and organs are separated from other organs and from the environment by membranes as well. Each of these membranes has evolved to have different transporters to control the distribution of biologically relevant species among these compartments. Some of these transporters are nanopores (length commensurable with radius) and nanochannels (length much larger than radius): ion channels [1–6] and ion pumps [3] are examples of the latter while and nuclear pores complexes [7–9] represent the former. The understanding of the fundamental characteristics of biological nanopores and nanochannels, their transport and gating characteristics, provides for design guidelines for synthetic nanopores. The challenging question that arises is how one can design synthetic mimics of nanopores, that share some of the advantages of their biological counterparts (such as biochemical selectivity, control over transport direction and response to external stimuli), while their molecular compositions and environments are much simpler.

The exquisite control of biological ion channels and pores arises from the formation of cavities with size and charge selectivity that can be tuned by conformational changes of the protein pores or by a molecular reorganization of disordered proteins in the case of nuclear pore complexes. These capabilities are unique to proteins that have been developed through long evolutionary processes, either through changes in secondary structure or through molecular reorganization enabled by specific sequences in disordered proteins (proteins with no secondary structure). It is important to emphasize that biological systems are selective due to their ability to tune the environment on top of their use of specific molecules. This combination of specific molecular structures and environment is not very well understood and therefore biomimetic systems lack the flexibility of natural ones. However, as we progress in our understanding, we expect to be more capable of tuning synthetic systems and their surroundings to provide optimal activity and responsiveness. We review here some examples of

*Corresponding author: Szleifer, I. (igalsz@northwestern.edu)

1369-7021/Published by Elsevier Ltd. http://dx.doi.org/10.1016/j.mattod.2014.10.020

Please cite this article in press as: M. Tagliazucchi, I. Szleifer, Mater. Today (2014), http://dx.doi.org/10.1016/j.mattod.2014.10.020

synthetic nanopores and channels that have capabilities inspired by biological systems and discuss their advantages, limitations and ideas for future developments. This work is not intended to be an exhaustive review of transport in nanopores and nanochannels. We rather aim to critically discuss the general mechanisms of bioinspired transport, survey some state-of-the-art experimental accomplishments and identify future challenges for modeling and experiments. We refer the reader to some recent reviews in the field [10–20] to expand on some of the topics covered here. We will rely on theoretical and modeling results for a fundamental understanding of the transport mechanism in synthetic pores.

Fundamentals of electrically driven transport

In this section, we introduce some concepts about nanopores and nanochannels that will be useful in the discussion of bioinspired transport. Figure 1a shows a scheme of a channel that connects two reservoirs of identical composition and that has positively charged inner walls. When a charged surface is immersed into an electrolyte solution, ions of opposite charge are attracted to it, thereby forming an electrical double layer [21]. The thickness of this double layer is dictated (in the linear regime) by the Debye length of the solution, which characterizes the length scale of the electrostatic screening between the charged species due to the finite concentration in the solution. If the radius of the channel is much larger than the Debye length (which is typically in the nanometer range, e.g. 1 nm for a 0.1 M 1:1 electrolyte), then anions accumulate close to the inner wall, but cations and anions have the same concentration in the center of the channel. On the other hand, if the radius of the channel is shorter than the Debye length (i.e. a nanochannel), then the concentration of anions is much larger than that of cations everywhere within the channel. The concentrations of both ions in this last example are depicted in Fig. 1b.

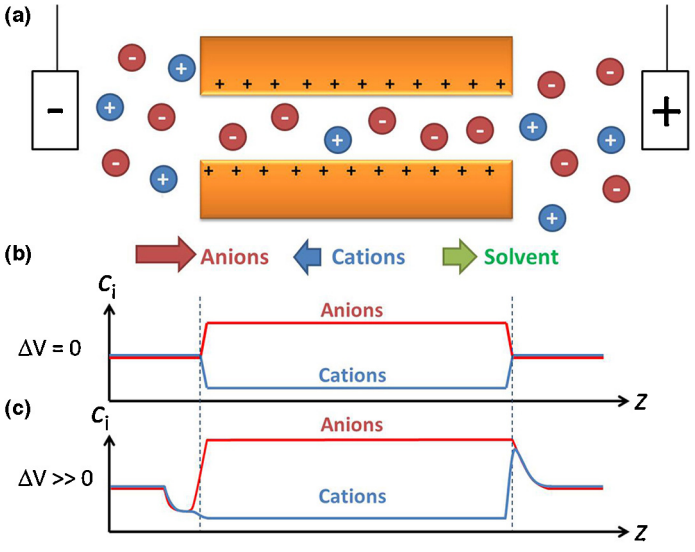

FIGURE 1

(a) Scheme of a channel connecting two reservoirs. The inner walls of the nanochannel are positively charged and, therefore, the concentration of anions in the inner solution is larger than in the reservoirs. The arrows show the direction of ion and solvent fluxes upon applying a potential difference between the reservoirs as shown in the scheme. (b, c) Concentration of anions and cations along the axis of the channel in equilibrium (panel b, no applied bias, $\Delta V = 0$) and for a large applied potential (panel c).

Let us now consider the effect of applying an electrical potential to reversible electrodes located in the reservoirs. In these conditions, anions will flow toward the positive electrode and cations toward the negative one. The nanochannel of the figure conducts almost exclusively anions and, therefore, the current carried by the anions is much larger than that carried by the cations (i.e. the channel is anion permselective). As the ions move due to the applied potential, they collide with solvent molecules and transfer momenta to them. In the case of Fig. 1a, the anions are the majority charge carrier and, therefore, they drag the solvent molecules toward the positive electrode. This electrically driven flux of solvent is known as electroosmotic flow.

For large applied potentials, the concentration of ions in the steady state deviates from that in equilibrium. In the case of the example in Fig. 1a the concentration of anions inside the channel is larger than in the reservoirs, therefore, the anions inside the channel can sustain a larger current that those in the entrance and exit of the channel. As a result, anions deplete near the entrance of the channel in the left reservoir and accumulate at the exit of the channel in the right reservoir (scheme of concentrations in Fig. 1c). The concentration of cations in the entrance and exit of the channel is similar to that of the anions due to electroneutrality requirements. The creation of depletion and accumulation regions at the mouths of the channel due to the applied potential is known as polarization concentration [22] and it causes the current-potential curves to deviate from linear, ohmic, behavior. The polarization concentration effects put in evidence the coupling that exists between structure and transport in nanochannels and it is responsible for current rectification in channels with broken symmetry. We will return to these topics later in this review.

The general equations that govern ion transport in nanopores and nanochannels are well established. The flux of ions obeys (within the linear response regime) the generalized diffusion equation:

$$\mathbf{J}_i(\mathbf{r}) = -D_i\rho_i(\mathbf{r})\nabla\beta\mu_i(\mathbf{r}) \quad (1)$$

where $\mathbf{J}_i$, D_i, ρ_i and μ_i are the flux, the diffusion coefficient, density and chemical potential of the ion i, $\beta = 1/k_BT$ and $\mathbf{r}$ denotes the position within the system. The chemical potential μ_i can be divided in an ideal component due to the translational (mixing) entropy of the ions and additional contributions due to the forces acting on the ions. These forces include osmotic, magnetic and electrostatic forces as well as interparticle interactions. In the nanofluidic literature, it is common to consider only the electrostatic contributions, which yields

$$\mu_i(\mathbf{r}) = \ln(\rho_i(\mathbf{r})\nu_w) + q_i\beta\psi(\mathbf{r}) \quad (2)$$

where ψ is the electrostatic potential, q_i is the charge of the ion i and ν_w is the molecular volume of the solvent. Combining Eqs. (1) and (2), with the mass conservation requirement leads to a generalized diffusion equation, which is known as the Nernst–Planck equation, i.e.

$$\frac{\partial\rho_i}{\partial t} = -\nabla\mathbf{J}_i(\mathbf{r}) = [\nabla(D_i\nabla\rho_i(\mathbf{r})) + \nabla(D_i\rho_i(\mathbf{r})q_i\nabla\beta\psi(\mathbf{r}))] \quad (3)$$

where the first term in the right hand side represents ideal Fick's diffusion and the second term accounts for the electrostatic interactions on the diffusion of the ions.

Please cite this article in press as: M. Tagliazucchi, I. Szleifer, Mater. Today (2014), http://dx.doi.org/10.1016/j.mattod.2014.10.020

The electrostatic potential is dictated by the Poisson equation:

$$\varepsilon\nabla^2\psi(\mathbf{r}) = -\rho_Q(\mathbf{r}) \quad (4)$$

where ρ_Q is the total charge density (i.e. the sum of the charge densities of all charged species) and ε is the dielectric constant. Eqs. (3) and (4) are known as the Poisson-Nernst–Planck equations.

The transfer of momenta between ions and solvent is dictated by the Navier–Stokes equation:

$$\rho\left(\frac{\partial\mathbf{v}}{\partial t} + \mathbf{v}\cdot\nabla\mathbf{v}\right) = -\nabla p + \eta\nabla^2\mathbf{v} + \mathbf{f} \quad (5)$$

where $\mathbf{v}$ is the velocity of the fluid, ρ is its mass density, p is the pressure, η is the viscosity of the fluid and $\mathbf{f}$ is the volume force acting on the fluid. This volume force may contain different contributions (e.g. gravitational, electrostatic and magnetic forces), but in the case of interest the most important contribution to $\mathbf{f}$ is the force that the electric field exerts on the ions in the fluid, namely $\mathbf{f} = -\rho_Q\nabla\psi$.

The set of Eqs. (3)–(5) (combined with the appropriated boundary conditions) has been widely used to model ion transport in many examples of solid-state nanochannels and nanopores [23–30]. Recent theoretical work has extended this fundamental description in other to describe, for example, systems with grafted polyelectrolytes [31–33]. It is important to note that Eqs. (3)–(5) provide a continuum description of the ion fluxes that is appropriate when the radius of the channel is larger than two times the Debye length [34–36]. Modeling of pores and channels with radii smaller than two Debye lengths, including most biological ion channels, requires particle-based methods, such as molecular or Langevine dynamics.

Chemically gated ion channels

Biological ion channels are very effective in discriminating between ions of opposite charge. Transport selectivity in ion channels relies on a constriction in the channel, known as the selectivity filter, which allows the passage of ions on a one-at-a-time basis. The presence of amino acids close to the selectivity filter with a charge opposite to that of the diffusing ion guarantees charge-selective transport [1]. Some types of ion channels can be opened and closed (gated) by chemical stimuli, such as glycine, acetylcholine, Zn^{2+} ions, glutamate, serotonin and γ-aminobutyric acid (GABA) [1,6,37]. Protons are the simplest chemical stimuli known to gate ion channels; examples of pH-switchable ion channels are the acid-sensing ion channels (ASICs) [38], the tetrameric M2 protein from influenza A [39] and the K^+ channel Slo3 from mammalian spermatocytes [40].

We will start our discussion by analyzing a synthetic ion nanochannel that is gated by protons and that displays a large charge selectivity [41]. This nanochannel (Fig. 2a) has a diameter of 15 nm and its inner walls are modified by a layer of end-grafted poly(4-vinyl pyridine), 4PVP, a weak polybase. The fraction of charged 4PVP segments in the system can be switched by the external pH according to the following equation:

$$f = \frac{1}{1 + 10^{-\log_{10}[H^+]^{pore} - pK_a}} \quad (6)$$

where $[H^+]^{pore}$ is the concentration of protons inside the PVP layer within the pore. As we discuss below, this concentration differs from that in the bulk solution, which is dictated by the solution

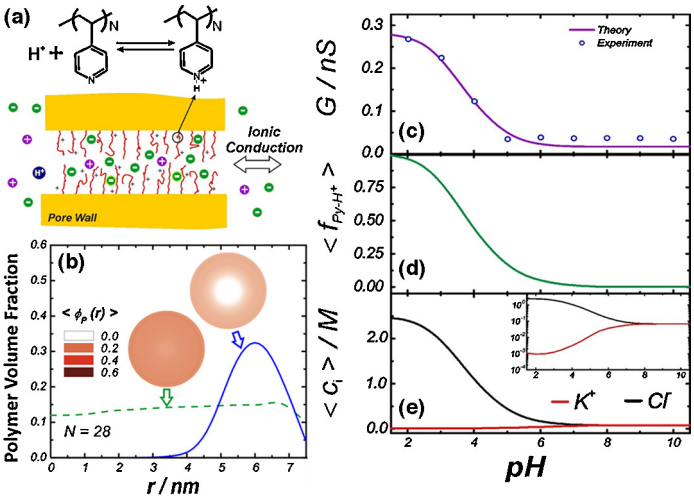

FIGURE 2

(a) Scheme of a nanochannel modified with end-tethered chains of poly(4-vynil pyridine), 4PVP. The pyridine segments in 4PVP can be either in a positively charged protonated state (pyridinium) or in a neutral deprotonated state (pyridine). The population of these two states is regulated by an acid-base equilibrium. The channel is connected to two identical macroscopic reservoirs containing 0.1 M KCl and fixed pH. An ion current results upon applying an electric potential difference between the reservoirs. (b) Polymer volume fraction as a function of the distance from the pore center (r) for pH 2 (charged polyelectrolyte, dashed green line) and pH 10 (neutral polyelectrolyte, solid blue line). The color maps show the polymer distribution across a plane perpendicular to the axis of the pore. (c) pH dependence of the conductance of the nanochannel. The symbols show the experimental conductivity from Yameen *et al.* [41] and the solid line show the theoretical prediction [32]. (d) Fraction of protonated segments averaged inside the channel. (e) Concentration of K^+ and Cl^- averaged inside the channel. The inset shows the concentrations in logarithmic scale. Reproduced and adapted with permission from Ref. [32]. Copyright 2010 American Chemical Society.

pH, due to the effect of the local environment within the pore. In general, $[H^+]^{pore}$ changes non-linearly with the bulk pH [42]; therefore while Eq. (6) has the same form as the equation for the titration of an acid in the bulk solution, the shape of the f vs bulk pH curve may be very different from an ideal titration curve. It is useful to define an apparent pK_a (pK_a^{app}) as the bulk pH for which $f = 0.5$. Because of the effect of the local environment, the apparent pK_a and the pK_a in bulk solution may be very different [16].

The nanochannel of Fig. 2 connects two reservoirs containing KCl 0.1 M solutions of a given pH. An ionic current flows through the channel upon applying a potential bias between these reservoirs. The points in Fig. 2c show the conductance of the channel as a function of the pH in the reservoirs as measured by Yameen *et al.* [41]. The conductance of the channel is low in basic pH solutions and increases around pH 3.8, which demonstrates conductivity gating by protons. To understand the mechanism behind this effect, we studied the system with a molecular theory, which explicitly considers the properties of the molecules in the system (e.g. their charge, conformations and size) and their inter and intramolecular interactions (e.g. electrostatic, hydrophobic and excluded-volume interactions) [32]. The theory provides structural and thermodynamic information on the system. Figure 2b shows the volume fraction (i.e. density) of the 4PVP as a function of the

Please cite this article in press as: M. Tagliazucchi, I. Szleifer, Mater. Today (2014), http://dx.doi.org/10.1016/j.mattod.2014.10.020

distance from the wall of the nanochannel for pH 2 (the *open* conductivity state) and pH 10 (the *close* conductivity state). At pH 2, the 4PVP chains are charged and therefore adopt rod-like conformations, reaching the center of the channel. At pH 10, the chains are uncharged and they collapse on the channel walls due to the hydrophobic interactions among pyridine segments [43]. Therefore, the polymer is homogeneously distributed inside the nanochannel in the *open* conductivity state, whereas the axis of the channel is free of polymer segments in the *close* state. This result indicates that pH-induced gating is not related to the structural reorganization of the 4PVP layer.

Figure 2d shows that the average protonation state of the channel (i.e. the value of f given by Eq. (6)) shows the same dependence on the solution pH as the conductance. The relationship between the protonation fraction of the 4PVP and the conductance becomes clear when we consider the average concentration of cations and anions inside the nanochannel (Fig. 2e): at low pH, anions enter the channel to compensate the charge of the protonated 4PVP. The predicted concentration of anions at this pH is >2 M and, therefore, the total concentration of ions is much larger at low pH than at high pH. The conductance is directly proportional to the concentration of ions inside the channel, which explains the mechanism of pH-induced gating. In fact, the conductivity of the channel as a function of pH predicted by the molecular theory (solid line in Fig. 2c) is in excellent agreement with the experimental results [32]. It is interesting to note that the apparent pK_a observed in Fig. 2d is 3.8 (i.e. this is the pH where half of the pyridine groups in the nanochannel are protonated), while the pK_a of pyridine in the bulk is 5.2. The pK_a^{app} is smaller than the bulk pK_a because the positive electrostatic environment inside the nanochannel excludes protons from it, and, therefore, the pH required to protonate half of the pyridines inside the channel is smaller than that required for pyridines in the bulk solution. Loosely speaking, the shift of the pK_a of the pyridine species inside the pore is as a local Le Chattelier principle: the positive charges of the 4PVP shift the acid-base equilibrium from the positively charged species (pyridinium) toward the neutral species (pyridine) and, thus, the bulk pH required to protonate half of the pyridines inside the pore is lower than the pK_a for a pyridine in solution. In other words, the repulsive electrostatic interactions within the pore shift the titration curve. Namely, the chemical free energy cost of shifting the acid-base equilibrium is compensated by the reduction in electrostatic repulsion that results from reducing the charge in the confined polymers. This charge regulation effect not only affects nanochannels modified by pH-responsive polyelectrolytes but also systems where the inner walls have weak acid or basic groups. The later situation was analyzed by Yeh *et al*. using numerical calculations [44] and analytical theory [45]. These works showed that charge regulation is coupled to the polarization concentration effect, which results in gradients of pH and degree of protonation along the axis of the pore [44].

Figure 2e shows that the charge carriers inside the nanochannel at low pH are almost exclusively Cl^- ions and, hence, the anion selectivity (current carried by the anions over the total current) is very high. Theory predicts an ionic selectivity (IS) of 0.994 for the channel in Fig. 2 [32]. This selectivity is higher than the value of IS ~0.7 predicted for nanochannels with inner surfaces modified by surface charges [24] and it is comparable to the ion selectivities of biological ion channels, such as glycine (IS ~0.97) and GABA (IS ~1) anion-selective channels and the serotonin cation-selective channel (IS ~0.98) [6,37]. The predicted large ion selectivity of polyelectrolyte-brush modified nanochannels, which should be experimentally confirmed in the future, arises from the large charge density immobilized by the polyelectrolyte brush inside the pore, which is much larger than that achievable by surface charges. Note that while the ion selectivity of the synthetic channel is similar to biological ion channels, the mechanism responsible for this behavior is different in each case. Moreover, the synthetic systems are selective in the transport of cations versus anions, while their biological counterparts are able to also select between different types of ions of the same charge, as discussed below.

Electrostatic modulation of nanochannel conductivity is not restricted to gating by protons. In principle, any process able to modify the charge on the walls of the channel can be used for gating, for example electrostatic gating was achieved in phosphate-modified pores by Ca^{2+} addition [46,47] and in photoacid-modified channels by light [48,49]. It is worthwhile to note, however, that gating in biological channels do not rely on the electrostatic gating mechanism discussed so far. Gating in biological ion channels occurs when agonists bind/unbind to sensor sites (which may be far from the channel itself) and initiate a series of conformational changes that physically block the channel. A similar mechanism of gating by conformational rearrangement is found in some synthetic nanochannels, for example in those modified by the thermoresponsive polymer poly(isopropyl acrylamide) (pNIPAM) [50,51], which sterically blocks the pore in its hydrophilic state (low temperature) and opens the pore in its hydrophobic state by collapsing on the wall (high temperature). Blocking of ion flows by adsorption of large macromolecules is another possible mechanism to gate the conductance of synthetic channels [52–56]. For example, solid-state nanopores with inner walls modified by nitrilotriacetic acid receptors bind histidine ligands in proteins [52]. Binding events modify the current through the pore and allow stochastic sensing of the proteins. Interestingly, the binding/unbinding equilibrium of the proteins inside the channel depends on the presence of ion currents, since the non-equilibrium electric field sustained by these currents exerts a force on bound proteins that weakens the ligand-receptor bond. This example illustrates the coupling that exists between the transport of ions and the structure of the pore.

It is important to realize that blocking the conductance of synthetic nanochannels via conformational changes or adsorption of large molecules is rather inefficient. In general, the ratio of the conductivity in the *close* state to that in the *open* state is considerably smaller than that observed in biological channels. This inefficiency is a direct consequence of the nanometric diameter of solid-state channels, which is much larger than the size of a single ion.

Ion-selective channels

An important difference between biological and synthetic ion channels is that the former exhibit high selectivities toward the chemical identity of the translocating ion, for example potassium

Please cite this article in press as: M. Tagliazucchi, I. Szleifer, Mater. Today (2014), http://dx.doi.org/10.1016/j.mattod.2014.10.020

channels, such as the KcsA [57], can be ~10^3–10^4 more selective for K^+ than for Na^+. This selectivity is achieved by the presence of carbonyl oxygen atoms in the selectivity filter [57], which coordinate K^+ and Na^+ differently. To mimic the chemical selectivity of biological channels, the size of the synthetic pores must be commensurable with the diameter of the diffusing ions (~0.2–0.6 nm) and the pore walls should expose the proper chemical residues to interact selectively with the ions. Graphene pores and carbon nanotubes have emerged as one of the best candidates for chemically selective solid-state ion channels. For example, different alkaline ions permeate through intrinsic defects in graphene sheets with different rates [58]. Molecular dynamics (MD) simulations have been used to address selective transport in graphene membranes and carbon nanotubes with site-specific chemical functionalization. Sint *et al.* [59] studied graphene nanopores of 0.5 nm in diameter terminated either in N and F (Fig. 3a, left) or H (Fig. 3a, right) atoms. The N,F-terminated pore was selective to cations with a relative Li^+:Na^+:K^+ selectivity of 9:14:33; the H-terminated pore was anion selective with a F^-:Cl^-:Br^- selectivity of 0:17:33. Carbon nanotubes with inner surfaces modified by carbonyl residues (Fig. 3) also displayed selective transport of Na^+ and K^+ [60]; in this case, the selectivity depended on the arrangement of the carbonyl groups on the surface. Inspired by K^+ and Na^+ biological channels, He *et al.* [61] studied the translocation of Na^+ and K^+ through graphene nanopores terminated in carbonyl (Fig. 3c, 4CO) or carboxylate (Fig. 3c, 4COO and 3COO) groups. The pores modified by four carbonyl groups (Fig. 3c, 4CO) and by four carboxylates (Fig. 3c, 4COO) selectively transported K^+ and Na^+, respectively. The small pore modified by three carboxylates (Fig. 3c, 3COO) was selective to Na^+ at low applied voltages, for which Na^+ bound strongly to the pore and prevented K^+ translocation. However, at high applied voltages, Na^+ no longer blocked the pore and transport became K^+ selective. This example shows again the strong coupling between structure and transport in nanopores. It will be interesting to verify these predictions with experimental observations.

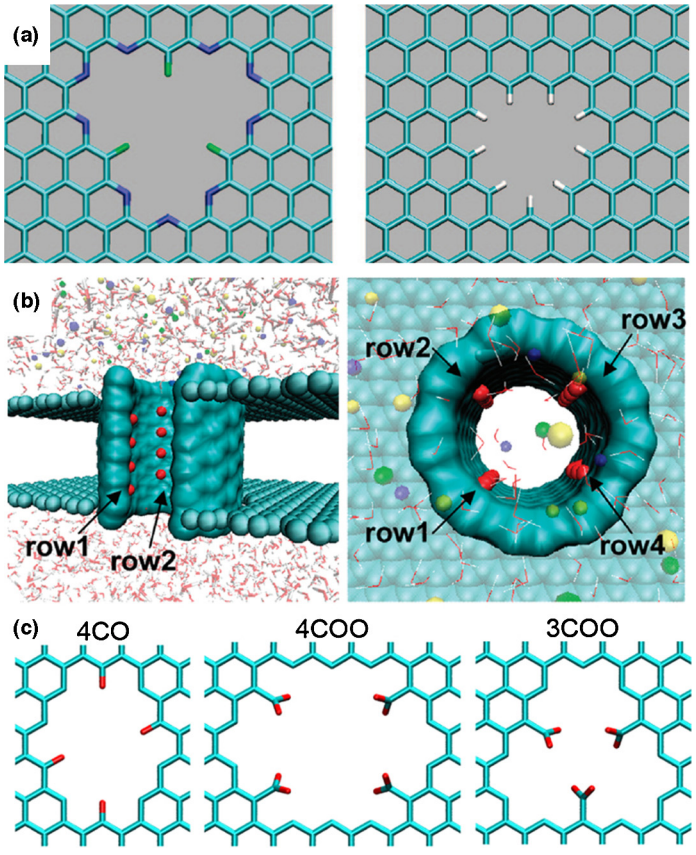

FIGURE 3

(a) Structure of graphene nanopores studied by MD simulations. The pores were terminated either in F or N (left) or H (right). The color of the atoms is as follows: cyan: C, blue: N, green: F, white: H. Reproduced from Ref. [59]. Copyright 2008 American Chemical Society. (b) Carbon nanochannel modified by carbonyl groups in a membrane studied by MD simulations. The color of the atoms is as follows: cyan: C, red: O (i.e. carbonyl groups), green: K^+, blue: Na^+, yellow: Cl^-. Reproduced from Ref. [60]. Copyright 2010 American Chemical Society. (c) Structure of graphene nanopores studied by MD simulations. The color of the atoms is as follows: cyan: C, red: O. Reproduced from Ref. [61]. Copyright 2013 American Chemical Society.

Current-rectifying pores and channels

The inward-rectifier potassium channels (Kir channels) are potassium-selective ion channels that transport ions into the cell much more easier than out of the cell [4]. Current-potential curves for these channels are non-ohmic (non-linear), see scheme in Fig. 4a. In other words, the current of Kir channels is large when the applied potential drives K^+ ions into the cell (negative applied potential in the scheme of Fig. 4a) and it is small when the potential (and therefore the direction of transport) is reversed. Current rectification requires breaking the symmetry of the channel with respect to the plane of the membrane, which in the case of Kir channels is achieved by the presence of cytoplasmic magnesium ions and polyamines that adsorb into the pore [62].

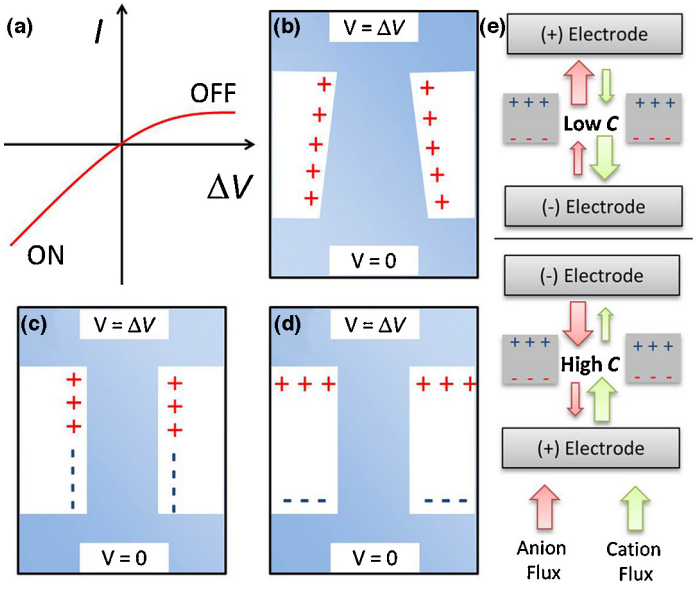

FIGURE 4

(a) Scheme of a typical current-potential curve for a current-rectifying nanochannel. Current rectification requires to break the symmetry of the system, for example by using non-cylindrical channels (b) or pores where the inner (c) or the outer (d) walls have charges of opposite sign on each half of the pore. Following the convention of the figure, the conductivity of the pore is higher for $\Delta V < 0$ (*open* state) than for $\Delta V > 0$ (*close* state). (e) Ion fluxes for the system in panel (d) showing the operation of the pore in the *off* state (upper panel) and the *on* state (bottom panel).

Please cite this article in press as: M. Tagliazucchi, I. Szleifer, Mater. Today (2014), http://dx.doi.org/10.1016/j.mattod.2014.10.020

Moreover, the cytoplasmic environment and the extracellular matrix present highly asymmetric solutions. In synthetic nanochannels connecting reservoirs with identical solutions, current rectification can be achieved by asymmetric nanopore shapes, such as conical pores [63–65] (Fig. 4b), or by having an asymmetric charge distribution in a shape-symmetric pore, for example in nanochannels whose inner [23,66–68] (Fig. 4c) or outer [23,31] (Fig. 4d) walls present charges of opposite sign on the upper and lower halves of the channel. Current rectification in these systems arises from changes in the concentration of ions inside the channels under an applied potential, whereas the specific details of the mechanism depend on the particular system. For example, current rectification in a nanopore with asymmetrically charged outer walls is exemplified in Fig. 4e. When the positively charged electrode faces the positive side of the membrane (upper panel in Fig. 4e), the cations enter the pore through the mouth with positively charged outer walls and exit it via the mouth with negatively charged outer walls. Since the entrance resistance is larger than the exit resistance, the cations are depleted inside the nanopore. The same argument applied to the anions shows that they also deplete inside the pore. The salt concentration inside the pore is therefore smaller than in the bulk and the channel is in its *off* state. When the positively charged electrode faces the negative side of the membrane (lower panel in Fig. 4e), the entrance resistance is lower than the exit one, ions accumulate inside the pore and the system is in its *on* state.

The transport properties of current-rectifying nanochannels can be gated by protons when the surface charges depend on the external pH, which can be the same or different in both reservoirs. The latter situation was studied experimentally by Ali *et al.* [27] and by Zhang *et al.* [68] using cigar-like nanochannels connecting reservoirs of different pH. The two ends of the nanochannel prepared by Zhang *et al.* [68] were functionalized by end-grafted 4PVP and poly(acrylic acid) (PAA) chains. The electrostatic gates created by the polyelectrolyte layer on each end of the channel can be addressed individually by the pH of the reservoir connected to that end. Hence, the PAA gate opens at pH 10 and closes at pH 2.8, while the 4PVP gate has the opposite behavior. The PVP/PAA gates allow, therefore, four different nanochannel states: *close*/*close*, *open*/*close*, *open*/*open* and *close*/*open* (Fig. 5a). In the *open*/*open* state,

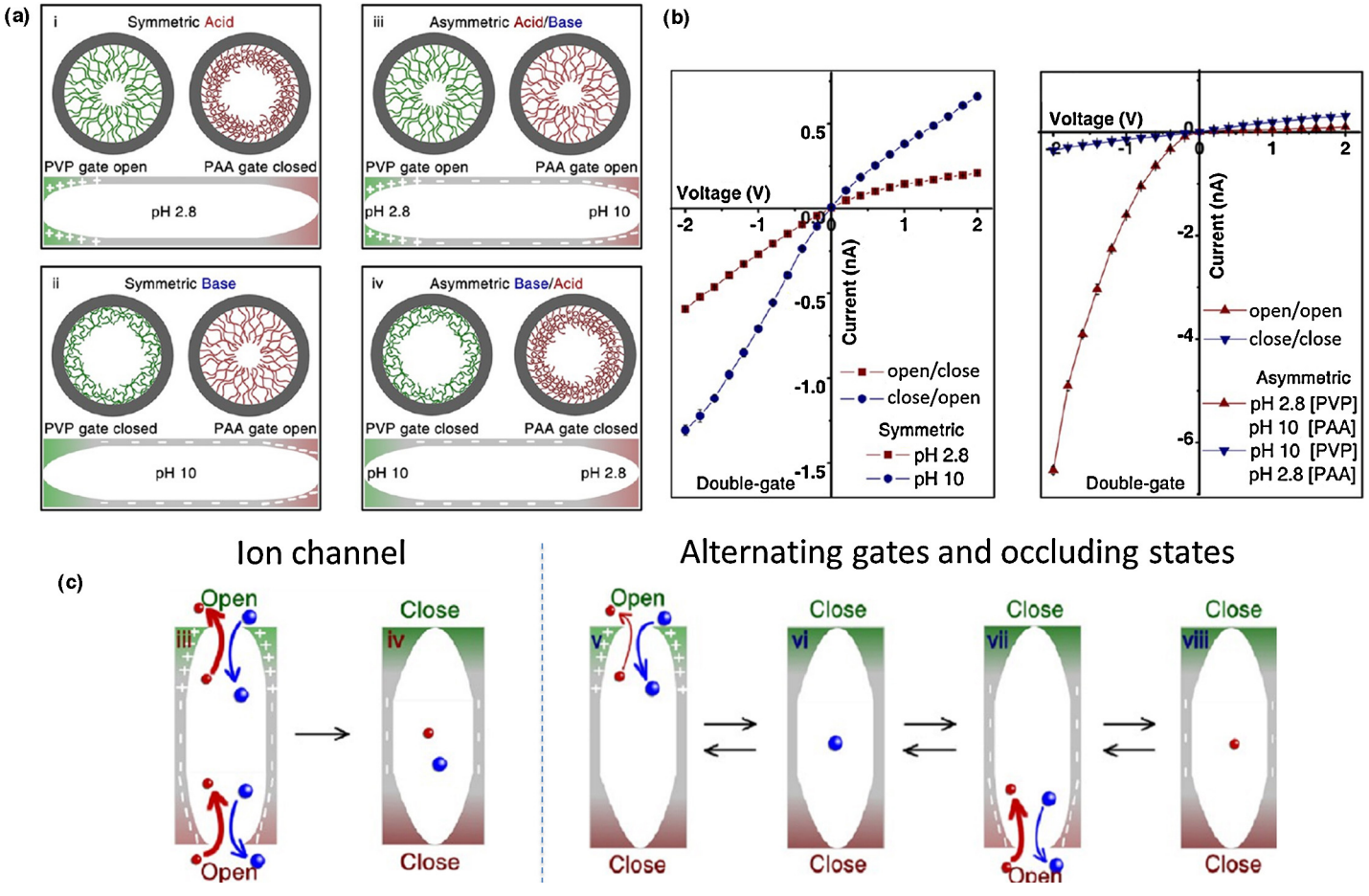

FIGURE 5

(a) Schemes showing the structure of a cigar-shaped nanochannel that has been modified with poly(vinyl-pyridine) (PVP) on one end and with poly(acrylic acid) (PAA) on the other for different combinations of pH in the left and right reservoirs. The PAA is in a stretched, charged and ion-conductive state at pH 10 (*open* state) and in a collapsed, neutral and non-conductive state at pH 2.8 (*close* state). The behavior of PVP is opposite to that of PAA: the PVP gate is *open* at pH 2.8 and *close* at pH 10. (b) Current–potential curves for the systems in a. Each curve corresponds to a different configuration of the PVP/PAA gate: *open*/*close* (left panel, red curve), *close*/*open* (left panel, blue curve), *open*/*open* (right panel, red curve) and *close*/*close* (right panel, blue curve). (c) Manually switching the pH of the reservoirs allows opening and closing the electrostatic gates at the ends of the pore. The 'ion channel' and 'alternating gates and occluding states' operation modes are discussed in the text. Reproduced and adapted with permission from Ref. [68]. Copyright 2013 American Chemical Society.

Please cite this article in press as: M. Tagliazucchi, I. Szleifer, Mater. Today (2014), http://dx.doi.org/10.1016/j.mattod.2014.10.020

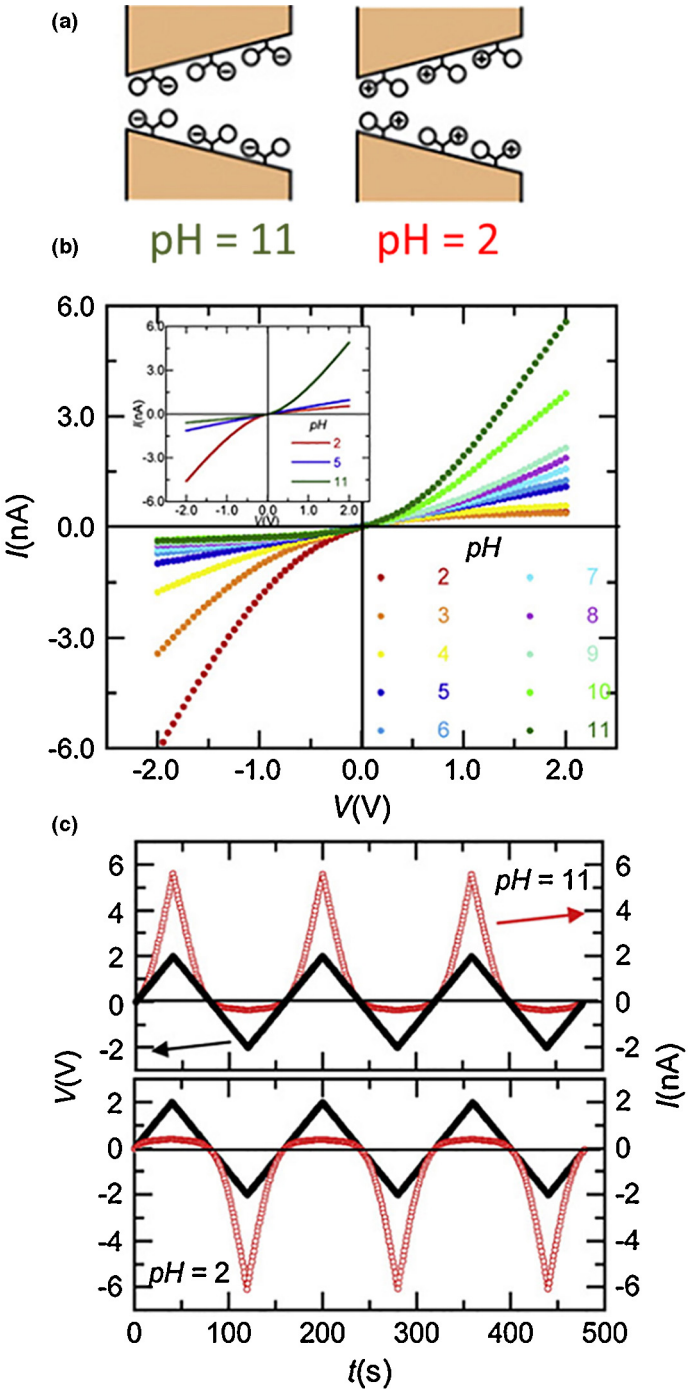

FIGURE 6

(a) Scheme of conical nanopores modified by amphoteric lysine groups, which are negatively charged at pH 11 and positively charged at pH 2. (b) Experimental current-potential curves obtained at different pH values for the system in a. Note that the pore rectifies ion currents in opposite directions at pH 11 and at pH 2. The inset shows the theoretical results at selected pH values. (c) Ionic current (red symbols) and applied potential bias (solid black line) as a function of time at pH 11 and pH 2. Note that due to current rectification there is a non-zero time-averaged ion current, even though the time average of the applied bias is zero. Reproduced and adapted with permission from Ref. [71]. Copyright 2013 Elsevier.

the charge asymmetry of the system is largest and the pore is highly rectifying (red curve in the right panel of Fig. 5b). In the *close*/*close* configuration, the channel is symmetric and the current is small and ohmic (blue curve in the left panel of Fig. 5b). Finally,

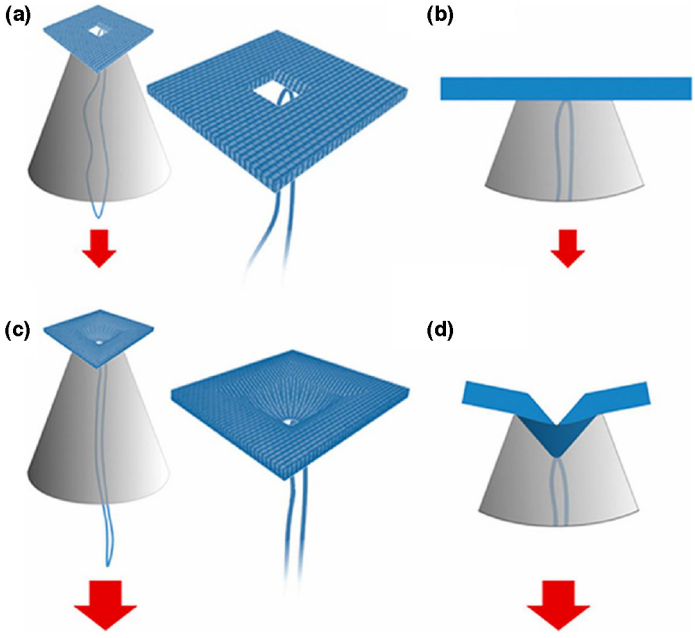

FIGURE 7

Scheme showing the voltage-dependent shape of DNA-origami-modified glass nanopores. (a, b) Flat conformation (low voltage), and (c, d) buckled conformation (high voltage). Reproduced and adapted with permission from Ref. [75]. Copyright 2014 American Chemical Society.

in the *open*/*close* and *close*/*open* states the channel rectifies current, but to a lesser degree than for the *open*/*open* configuration (right panel of Fig. 5b). For an applied bias of −2 V, the *open*/*open* and *close*/*close* states correspond to high and low conductance states, respectively, and switching between these states mimics the operation of an ion channel (Fig. 5c).

Ion pumps

Ion channels transport ions across membranes in the direction of the gradient of their electrochemical potentials (chemical potentials of charged species), which depend on both the concentration of the ions and the trans-membrane electrostatic potential. On the other hand, ion pumps force ions to move up their electrochemical potential gradient, consuming energy in the process. Structurally, ion pumps and channels differ in the number of gates: channels have a single gate, which can be either open or close, while pumps require two synchronized gates to drive ions against their electrochemical potential gradient [3]. The gates of the nanochannel of Fig. 5 can be switched in the order *open*/*close* → *close*/*close* → *close*/*open* → *close*/*close* (Fig. 5c, right panel) to resemble the operation of an ion pump. However, there are some important differences in the function of biological ion pumps and this synthetic channel: (i) the synthetic nanochannel does not really operate as a truly ion pump because no net flux of ions occurs against their gradient of electrochemical potential and (ii) the electrostatic gates in the nanochannel are not effective enough to allow fail-safe transport of ions. In their *close*/*close* (occluding) state, biological ion pumps tightly trap one or more ions. In the synthetic nanochannel, however, the *close*/*close* state has a non-negligible current (~100 pA at −2 V, according to Fig. 5b). This current carries 3×10^{10} ions per minute (which is the duration of each pH step in the experiment of Fig. 5c) across the channel.

Please cite this article in press as: M. Tagliazucchi, I. Szleifer, Mater. Today (2014), http://dx.doi.org/10.1016/j.mattod.2014.10.020

According to the dimensions of the nanochannel, its volume is $<0.1\ \mu m^3$ and, if filled with a 0.1 M electrolyte solution, it contains less than 10^7 ions. Therefore, in 1 min the ions inside the pore are renewed >1000 times in the *close/close* state, which means that the synthetic channel is leaky and cannot really trap ions, as suggested by the stages VI and VIII of Fig. 5c. To achieve a truly 'fail-safe' ion pump, much faster pH oscillations would be required.

Based on the discussion above, we consider unlikely the development of nanometer ion-pumps mimicking the exact mechanism of biological ones. However, nanometric ion-pumps based on other mechanisms are still feasible. In a seminal work, Siwy and Fulinski reported a synthetic ion pump that operates far-from-equilibrium by applying an alternating-current (ac) electric field across a membrane containing a single conical nanopore with negatively charged outer walls [63,69]. This strategy for ion-pumping (which is equivalent to the tilting ratchet mechanism in the non-equilibrium literature [70]) has been recently extended to pH-responsive channels (Fig. 6) [71]. This study used conical pores coated with amphoteric lysine groups, which are positively charged at pH 2 and negatively charged at pH 11 (Fig. 6a). At pH 2 or 11, the channel is both ion selective and rectifying (Fig. 6b). Therefore, upon applying an ac electric field, there is a net average flux of ions across the membrane (red points in Fig. 6c) despite the fact that the time-average of the electric field is zero (black lines in Fig. 6c). In this example, the solution pH determines the selectivity and directionality of the ion pump.

Another mechanism for uphill ion transport involves coupling it to the downhill transport of other species, in such way that the total change in free energy involved in the transport process is negative. This mechanism is the basis of some biological ion pumps, such as the calcium-sodium exchanger [72], and it has been recently applied to build a synthetic light-driven proton pump using a selective membrane [73]. However, to the best of our knowledge, synthetic nanopore or nanochannel pumps based on coupled ion transport have not been reported.

Voltage-dependent nanopores

Transmission of nerve impulses depends on voltage-dependent ion channels, whose permeability can be gated by changes in the trans-membrane potential. This switching mechanism involves a voltage-sensor domain that undergoes conformational changes induced by the transmembrane potential and that triggers conductivity changes [1,5,74]. We are far from understanding and mimicking this exquisite degree of molecular control; however,

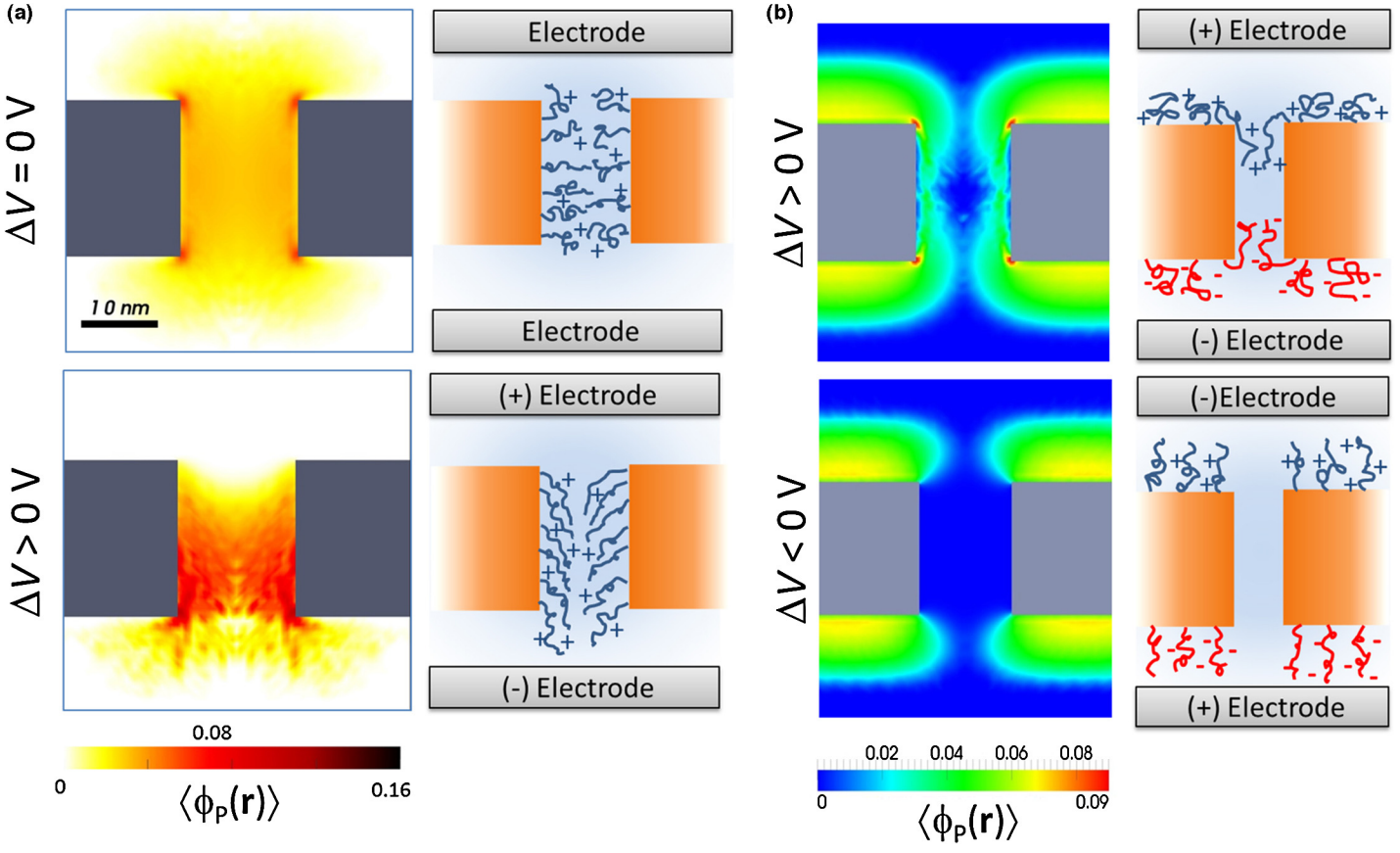

FIGURE 8

(a) Theoretical prediction of the polymer volume fraction (shown as color maps) for a short nanopore with an inner surface modified by positively charged polyelectrolytes. In equilibrium ($\Delta V = 0$, upper panel), the polymer is distributed symmetrically. Upon applying a positive potential bias to the upper electrode ($\Delta V = 0$, lower panel), the polyelectrolyte chains stretch toward the lower (negatively biased) reservoir. Reproduced and adapted with permission from Ref. [33]. Copyright 2011 American Chemical Society. (b) Same as (a) but for a short nanopore with upper and lower outer membrane surfaces modified by positively and negatively charged polyelectrolyte brushes, respectively. Upon applying a potential bias, electrophoretic forces stretch the grafted polyelectrolyte chains toward the oppositely charged electrodes. Therefore, the chains stretch into the pore for $\Delta V > 0$ (upper panel) and out from the pore for $\Delta V < 0$ (upper panel). Reproduced and adapted with permission from Ref. [31]. Copyright 2013 American Chemical Society.

Please cite this article in press as: M. Tagliazucchi, I. Szleifer, Mater. Today (2014), http://dx.doi.org/10.1016/j.mattod.2014.10.020

it is interesting to note that the structure of synthetic channels modified by soft materials is also sensitive to the trans-membrane potential and that potential-induced conformational changes can affect the conductance of the nanochannel.

Recent work by the Keyser [75] and Dekker [76] groups shows interesting voltage-dependent conductivity changes in nanopores modified by DNA-origamis (a DNA-origami is a nanostructure created by directed folding of DNA). For example, DNA-origami caps bearing a central aperture and dangling tails were trapped at the entrance of a glass nanopore under a positive applied potential bias. Depending on the magnitude of this applied potential, the caps adopted either a flat (Fig. 7a and b) or a buckled (Fig. 7c and d) conformation [75]. The buckled conformation was obtained for large applied potentials, which pulled the DNA dangling tails into the pore and, thus, deformed the DNA origami. This state had a lower conductivity than the flat one, since the buckled DNA origami sealed the glass pore better than the flat cap. The flat/buckled transition has been used to control the translocation frequency of ds-DNA chains through the pores [75].

Nanopores modified by end-grafted chain-like molecules also display potential-gated conformational changes. Harrell *et al.* proposed that the potential-driven reorganization of end-grafted DNA chains in conical nanopores worked as an electromechanical gate, which rectified ion currents [77]. We recently studied the voltage-induced reorganization of polyelectrolyte chains end-grafted in short nanopores using a non-equilibrium molecular theory [31,33]. Figure 8a shows the structure of a short pore whose inner surface is modified by end-grafted polyelectrolyte chains. The positively charged polyelectrolyte chains are distributed symmetrically in the absence of an applied bias (equilibrium), but, upon applying a potential bias, they deform toward the negative electrode [33]. This deformation changes the conductivity of the system and, hence, gives rise to non-linear current-potential curves [33]. We also studied theoretically the reorganization of a pore whose outer walls are modified by polyelectrolyte brushes of opposite charge, Fig. 7b [31]. Applying a positive bias to this system pulls the polyelectrolyte chains out of the pore (bottom panel). On the other hand, under a negative applied potential, the polyelectrolyte chains stretch into the pore, blocking it (upper panel). Free-energy calculations for the translocation of particles through this pore suggest that potential-induced deformation of grafted polyelectrolytes can act as an electrochemical gate to control the translocation of nanoparticles or macromolecules [31].

There are two important insights to be gained from our discussion of voltage-responsive synthetic nanopores. First, the mechanisms of gating of the synthetic channels and those of biological ion channels are qualitatively different. In biology, the trans-membrane potential triggers conformational changes of the sensor domain in the absence of ionic currents. On the other hand, in the synthetic channels, ionic currents are required to sustain a non-equilibrium electric field inside the pore, which is responsible for the deformation of the DNA origami or the polyelectrolyte chains (one can imagine this deformation as an electrophoretic force acting on the immobilized polyelectrolytes). In other words, no reorganization of the soft-material component would occur in the absence of ionic currents (e.g. if the potential bias is applied to ideally polarizable electrodes). The second important insight is the interplay between structure and transport. Figures 7 and 8 show that the molecular organization of soft-matter-modified nanopores is affected by the magnitude and direction of ion currents. At the same time, the structure of these pores dictates the conductance of the system, which reveals the coupling that exists between ion transport and structure. This coupling is also found in biological channels and pumps, for instance conformational changes and

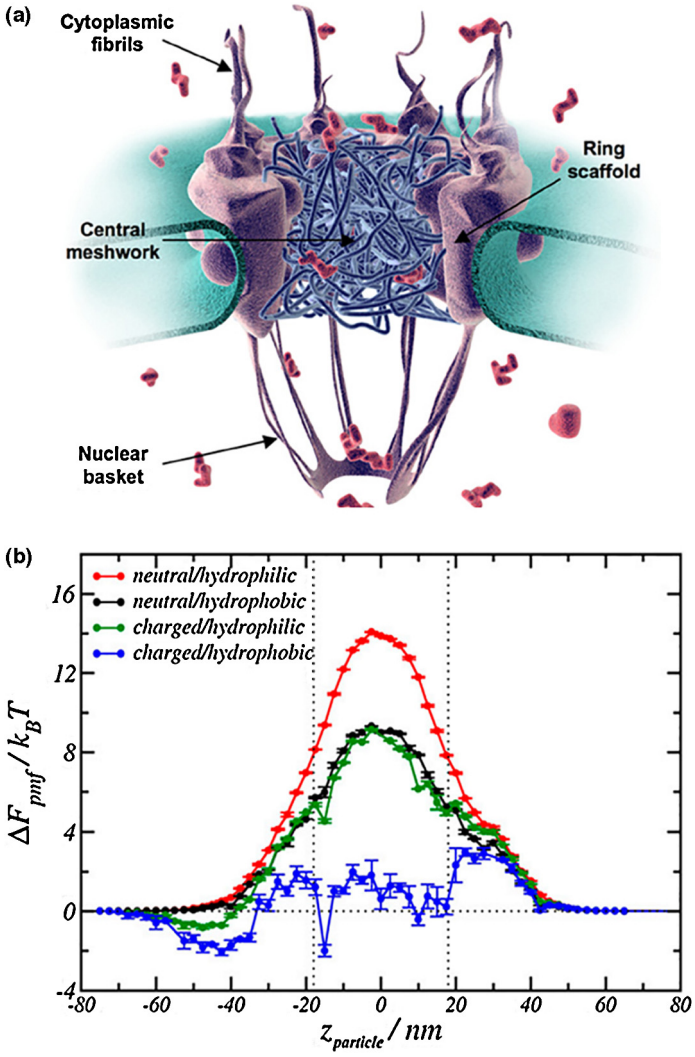

FIGURE 9

(a) Scheme of the nuclear pore complex (NPC), a protein complex in the nuclear membrane that controls all transport between the cytoplasm and the cell nucleus. The NPC has a diameter of ~50–100 nm (depending on the species) and its central meshwork is formed by disordered protein chains rich in phenylalanine-glycine motifs (the FG-Nups). The NPC blocks the passage to cargoes larger than 40 kDa in mass unless these cargoes are conjugated to transportins, which are hydrophobic and negatively charged proteins. Reproduced and adapted with permission from Patel *et al.*, Cell 2007, 129, 83. Copyright 2007 Elsevier Inc. (b) Free energy as a function of the position for a 10-nm spherical model particle translocating through the yeast NPC calculated with a molecular theory. Four different particles were considered depending on their charge and hydrophobic properties: the particles may be uncharged (neutral particle) or have a charge of $-150\ |e|$ (charged particle); they also may interact attractively with hydrophobic amino acids of the FG-Nups (hydrophobic particle) or not (hydrophilic particle). The center of the pore is located at $z = 0$ and the cytoplasmic and nuclear bulk solutions are located at $z \to \infty$ and $z \to -\infty$, respectively. Reproduced and adapted with permission from Ref. [80]. Copyright 2013 National Academy of Sciences.

Please cite this article in press as: M. Tagliazucchi, I. Szleifer, Mater. Today (2014), http://dx.doi.org/10.1016/j.mattod.2014.10.020

ion transport in ion pumps are two simultaneous and inseparable processes [3]. Thus, while structural changes are linked to ion transport in both biological and synthetic systems, the mechanisms responsible for these processes are qualitatively different.

Transport of cargoes larger than ions

The transport of cargoes larger than ions, such as molecules [18], polymers [78] or nanoparticles [30,79], through nanopores and nanochannels has been studied comprehensibly. So, can we learn something new from Nature? We believe that the answer to this question may reside in the outstanding selectivity of the nuclear pore complex, one of the most impressive examples of biological machinery. The nuclear pore complex (NPC, Fig. 9a) is a highly conserved biological nanopore in the nuclear membrane that mediates all cellular traffic between the cell nucleus and the cytoplasm. While small molecules (<40 kDa) can translocate easily through the NPC, larger cargoes require binding to specific proteins known as transport receptors or Karyopherins (Kaps) to be transported. It is still under debate how the Kap-cargo complex (which is larger than the cargo itself) can translocate through the NPC, while the cargo is blocked. It is accepted, however, that the selectivity of the NPC is granted by disordered proteins that protrude from the inner walls of the pore scaffold, see Fig. 9a. These proteins are known as FG-Nups due to their high content of phenylalanine (F)-glycine (G) motifs. We recently developed the first theory and computational model of the NPC that explicitly considered the size and shape of the pore, the amino acid sequence of the NPC, the size, charge and conformations of all molecular species involved in the system as well as the electrostatic and non-electrostatic interactions and the acid-base properties of the amino acid segments [80]. We used this model to study the translocation of spherical model nanoparticles having different surface hydrophobicities and charge densities. Figure 9b shows the free energy of the system as a function of the position of the particle along the axis. Free-energy curves for four different types of particles are shown: hydrophilic/neutral,

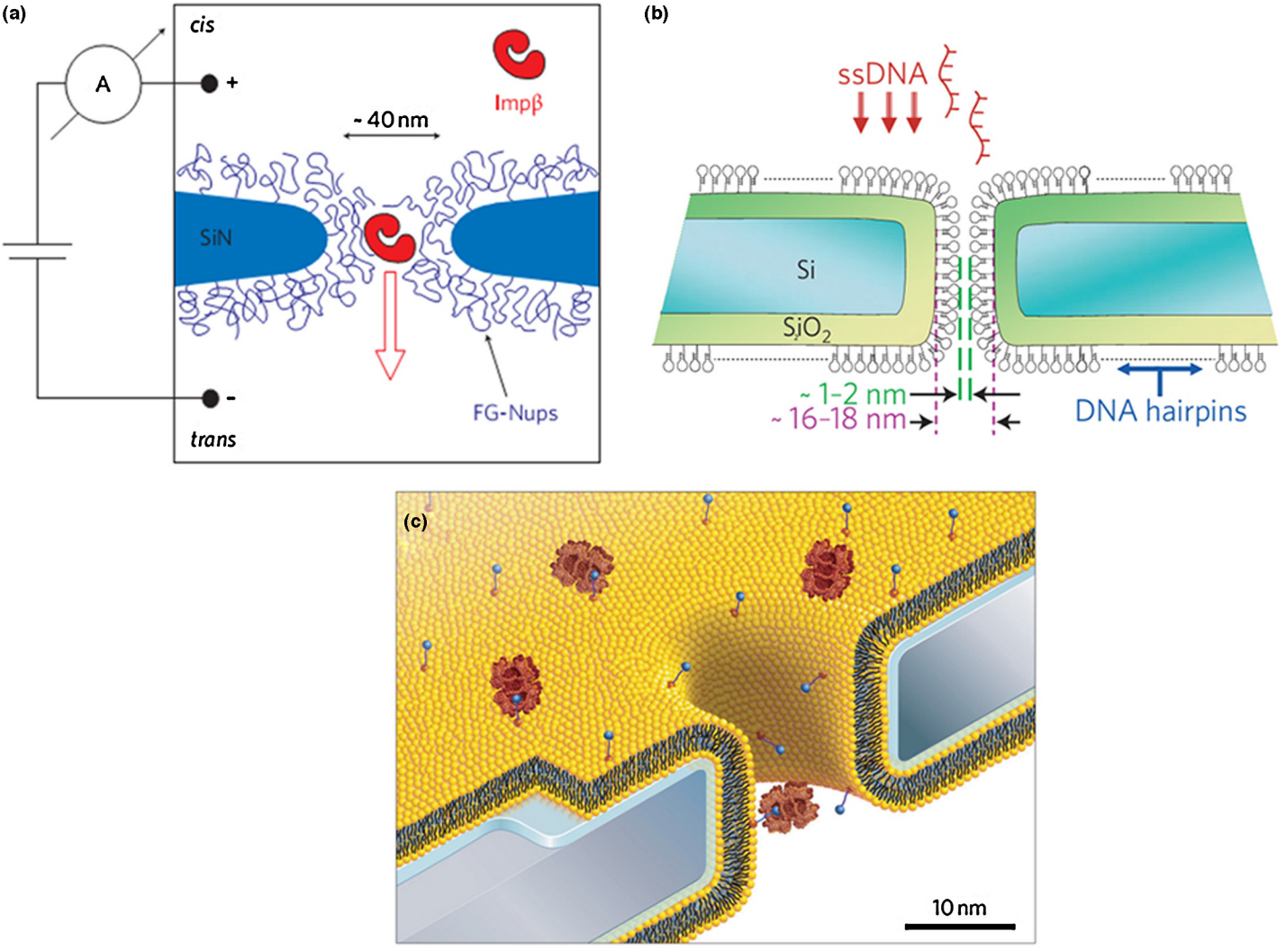

FIGURE 10

Examples of solid-state pores modified by biomaterials for selective transport of large cargoes: (a) solid-state nanopore modified by FG-Nups. Reproduced and adapted with permission from Ref. [81]. Copyright 2011 Nature Publishing Group. (b) Solid-state nanopore modified with hair-pin DNA. Reproduced and adapted with permission from Ref. [83]. Copyright 2007 Nature Publishing Group. (c) Nanopore modified with lipid bilayers incorporating ligand-modified lipids for selective transport. Reproduced and adapted with permission from Ref. [84]. Copyright 2011 Nature Publishing Group.

Please cite this article in press as: M. Tagliazucchi, I. Szleifer, Mater. Today (2014), http://dx.doi.org/10.1016/j.mattod.2014.10.020

hydrophilic/negatively charged, hydrophobic/neutral and hydrophobic/negatively charged. The hydrophilic/neutral curve has a free energy barrier for translocation (due to the steric interaction between the particle and the Nups), which decreases when the surface of the particle is hydrophobic and negatively charged. Interestingly, the experimentally known transport receptors, which are proteins that bind to the cargoes and assist them to translocate through the NPC, are in fact negatively charged and highly hydrophobic proteins. We believe, therefore, that the interplay among electrostatic, hydrophobic and steric interactions plays an important role in the outstanding selectivity of the NPC. Noteworthy, the effects of charge and hydrophobicity in the NPC are synergistic: the barrier for hydrophilic/neutral particles decreases by 5 k_BT when making the particle hydrophobic (hydrophobic/neutral particle) and by 5 k_BT when making the particle charged (hydrophilic/negatively charged); however, making the particle both charged and hydrophobic (hydrophobic/negatively charged particle) decreases the barrier by 12 k_BT instead of the expected 10 k_BT. This non-additivity arises from the reorganization of the disordered proteins within the pore in the presence of the cargoes, which is different for the different types of cargo. This is another example of the coupling between transport and structure in nanopores with tethered polyelectrolyte gates. A better understanding of this non-additive interplay of interactions as well as other aspects involved in transport selectivity in the NPC will lead to synthetic nanopores selective to specific nanoparticles or macromolecules.

A lesson gained from the NPC is that selective transport of large cargoes can be achieved by the synergistic interplay among different interactions coupled to changes in molecular organization. This last point reflects the importance of using soft layers as surface modifiers. One route to achieve such subtle balance of chemical and physical forces is to modify the inner surfaces of synthetic pores with biological materials, such as polyelectrolytes, lipids, DNA or proteins. For example, synthetic pores have been modified by reconstituted FG-Nups [81,82] to create biomimetic NPCs. In one of these examples (Fig. 10a), Dekker and collaborators tethered FG-Nups to the surface of a solid-state nanopore and showed that the transport receptor importin-β translocated effectively through this biomimetic pore, while non-specific proteins were blocked. In another example, sequence-selective transport of DNA was achieved in solid-state nanopores modified by DNA hair-pins (Fig. 10b). In this case, DNA hair-pins bound selectively to complementary DNA strands in solution and only these complementary strands were transported through the pore under an applied bias [83]. Lipids bilayers were also used to confer selectivity to biomimetic solid-state nanopores [84] (Fig. 10c). The fluid lipid layer was proposed to prevent the adsorption of non-specific proteins. Moreover, when lipids modified to target certain biomolecules were incorporated into the lipid layer, selective translocation of these specific biomolecules was observed. The mechanisms of transport selectivity in all examples discussed in Fig. 10 and the NPC share some important similarities: (i) specific chemical/physical affinity is required between the translocating cargo and the soft/biomaterials modifying the inner surfaces of the pore, (ii) tethered soft/biomaterials prevent unspecific translocation through the pore and (iii) transport-enabled cargoes reorganize the inner structure of the nanopore during translocation.

Conclusions

We have reviewed the transport mechanisms through synthetic nanochannels and nanopores in solid-state membranes and compared them to those in biological ion channels, ion pumps and nuclear pore complexes. The fundamental and general insights that arise from our analysis are: (i) Transport and structure are coupled. It is well-established that structure dictates the transport properties of the nanopore. However, it is not always recognized that transport affects structure. We have shown that soft materials confined in nanopores change their structure due to the ionic currents flowing through the pore. The degree of protonation of weak acids or bases within a pore also depends on the presence of ionic currents or large charged molecules. The structural and compositional changes due to the flux of ions or large particles affect the transport process and, therefore, transport and structure are highly coupled. (ii) Transport selectivity can be achieved by a synergistic combination of interactions. We have shown, for example, that the effective interactions that control transport of particles in our model of the NPC can be tuned from repulsive to attractive by combining electrostatic and hydrophobic interactions and that this is a synergetic combination: hydrophobic/charged particles experience a lower translocation barrier than that expected from the predictions for hydrophobic/neutral and hydrophilic/charged particles. An open question is how to achieve transport selectivity by engineering the interactions between the channel and the species being transported. To address this problem, the modeling tools need to go beyond the traditional Nernst–Poisson–Planck approach, which considers only electrostatic interactions. For example methods reviewed here such as full-scale simulations (which are currently computational too costly in many cases) and molecular theories. (iii) Synthetic channels and pores resemble some of the transport behavior found in their biological counterparts, but there are fundamental differences between them. Biological and synthetic ion channels are fundamentally different because the size of the selectivity filter in the former is similar to the size of a single ion, while the narrowest solid-state channels and pores are a few nanometers wide. Therefore, synthetic channels lack, so far, the chemical selectivity and gating properties of their biological counterparts. Since transport against electrochemical gradients by ion pumps depends strongly on ion selectivity and channel gating, the function of ion pumps is challenging to mimic. It is worthwhile to mention that, whereas man-made nanochannels and nanopores in solid-state membranes cannot compete (yet) with the selectivity and functional complexity of natural ones, they are mechanically and chemically much more robust than their biological equivalents. Also, synthetic channels have larger conductances than biological ones, as expected from their larger diameters.

Nanopores and nanochannels will continue to attract the attention of researchers in forthcoming years. Broadening the spectrum of chemical and physical stimuli that can gate synthetic nanochannels will lead to new applications in sensing. A major challenge in the field will be to improve the size and chemical selectivity of synthetic ion channels; this goal may be achieved in the future by, for example, graphene nanopores. Recent experiments have already demonstrated size-selective transport in graphene nanopores [85]; however selective permeation of ions of similar size (such as Na^+ vs K^+) is still challenging. The simulation

Please cite this article in press as: M. Tagliazucchi, I. Szleifer, Mater. Today (2014), http://dx.doi.org/10.1016/j.mattod.2014.10.020

results in Fig. 3 suggest that ion-selective transport in nanoporous graphene and carbon nanotubes is physically possible, but very sensitive to the molecular arrangement of chemical groups around the pore. Therefore, breakthroughs in nanofabrication are still required to accomplish ion-selective graphene nanopores. Another important challenge in the field of biomimetic nanochannels is the creation of fully synthetic nanochannel pumps, capable of transporting ions or molecules against their gradient of electrochemical potential. In this case, mimicking Nature may not work in the nanoscale and, therefore, other strategies, such as far-from-equilibrium transport, will be required. Finally, highly selective and stimuli-responsive transport of nanometric particles and macromolecules remains also a standing challenge, which will benefit from a deeper mechanistic understanding of biological systems such as the NPC. Methodological breakthroughs delivering new theoretical tools to model the different aspects of ion, molecular and macromolecular transport are also needed, as the large sizes of synthetic nanochannels often preclude the use of atomistic simulations. It is clear that the fundamental understanding of functional nanopores requires the ability to predict/design how molecular organization, chemical state, physical interactions and ion transport couple within nanoconfined environments. The complexity of the challenges lying ahead undoubtedly requires the combination of experiment and theory and the inspiration provided by a deeper understanding of biological transport.

Acknowledgments

We would like to thank our collaborators in the field of nanopores and nanochannels. This material is based upon work supported as part of the NERC (Non-Equilibrium Research Center), an Energy Frontier Research Center funded by the U.S. Department of Energy, Office of Science, Office of Basic Energy Sciences under Award Number DE-SC0000989.

References

[1] Biological Membrane Ion Channels: Dynamics, Structure, and Applications, Springer, New York, 2007.
[2] T.E. DeCoursey, Comp. Physiol. 2 (2012) 1355.
[3] D.C. Gadsby, Nat. Rev. Mol. Cell Biol. 10 (2009) 344.
[4] Z. Lu, Annu. Rev. Physiol. 66 (2004) 103.
[5] F. Bezanilla, Physiol. Rev. 80 (2000) 555.
[6] A. Keramidas, et al. Prog. Biophys. Mol. Biol. 86 (2004) 161.
[7] O. Peleg, R.Y.H. Lim, Biol. Chem. 391 (2010) 719.
[8] J. Fernandez-Martinez, M.P. Rout, Curr. Opin. Cell Biol. 24 (2012) 92.
[9] A. Harel, D.J. Forbes, Nat. Cell Biol. 3 (2001) E267.
[10] W. Guo, et al. Acc. Chem. Res. 46 (2013) 2834.
[11] X. Hou, L. Jiang, ACS Nano. 3 (2009) 3339.
[12] C. Dekker, Nat. Nanotechnol. 2 (2007) 209.
[13] Z.S. Siwy, S. Howorka, Chem. Soc. Rev. 39 (2010) 1115.
[14] C.R. Martin, Z.S. Siwy, Science 317 (2007) 331.
[15] H. Daiguji, Chem. Soc. Rev. 39 (2010) 901.
[16] M. Tagliazucchi, I. Szleifer, Soft Matter 8 (2012) 7292.
[17] X. Hou, et al. Angew. Chem. Int. Ed. 51 (2012) 5296.
[18] H. Bayley, C.R. Martin, Chem. Rev. 100 (2000) 2575.
[19] D.H. Stoloff, M. Wanunu, Curr. Opin. Biotechnol. 24 (2013) 699.
[20] S.W. Kowalczyk, et al. Trends Biotechnol. 29 (2011) 607.
[21] A.J. Bard, L.R. Faulkner, Electrochemical Methods, 2nd ed., John Wiley and Sons, New York, 2001.
[22] R.B. Schoch, et al. Rev. Mod. Phys. 80 (2008) 839.
[23] I. Vlassiouk, et al. ACS Nano 2 (2008) 1589.
[24] I. Vlassiouk, et al. Nano Lett. 8 (2008) 1978.
[25] L.H. Yeh, et al. J. Phys. Chem. C 116 (2012) 8672.
[26] H. Daiguji, et al. Nano Lett. 4 (2004) 2315.
[27] M. Ali, et al. ACS Nano 6 (2012) 3631.
[28] J. Cervera, et al. Electrochim. Acta 56 (2011) 4504.
[29] J. Cervera, et al. Europhys. Lett. 71 (2005) 35.
[30] W.J. Lan, H.S. White, ACS Nano 6 (2012) 1757.
[31] M. Tagliazucchi, et al. ACS Nano 7 (2013) 9085.
[32] M. Tagliazucchi, et al. J. Am. Chem. Soc. 132 (2010) 12404.
[33] M. Tagliazucchi, et al. J. Am. Chem. Soc. 133 (2011) 17753.
[34] B. Corry, et al. Biophys. J. 78 (2000) 2364.
[35] G. Moy, et al. Biophys. J. 78 (2000) 2349.
[36] B. Corry, et al. Chem. Phys. Lett. 320 (2000) 35.
[37] M.L. Jensen, et al. J. Neurochem. 92 (2005) 217.
[38] J. Jasti, et al. Nature 449 (2007) 316.
[39] I. Kass, I.T. Arkin, Structure 13 (2005) 1789.
[40] M. Schreiber, et al. J. Biol. Chem. 273 (1998) 3509.
[41] B. Yameen, et al. Nano Lett. 9 (2009) 2788.
[42] M. Tagliazucchi, et al. Proc. Natl. Acad. Sci. U.S.A. 107 (2010) 5300.
[43] O. Peleg, et al. ACS Nano 5 (2011) 4737.
[44] L.H. Yeh, et al. Anal. Chem. 85 (2013) 7527.
[45] Y. Ma, et al. Electrochem. Commun. 43 (2014) 91.
[46] A. Brunsen, et al. Langmuir 28 (2012) 3583.
[47] M. Ali, et al. ACS Nano 6 (2012) 9247.
[48] G. Wang, et al. J. Am. Chem. Soc. 128 (2006) 13553.
[49] L. Wen, et al. Adv. Funct. Mater. 20 (2010) 2636.
[50] B. Yameen, et al. Small 5 (2009) 1287.
[51] W. Guo, et al. ChemPhysChem 11 (2010) 859.
[52] R.S. Wei, et al. Nat. Nanotechnol. 7 (2012) 257.
[53] M. Ali, et al. J. Am. Chem. Soc. 130 (2008) 16351.
[54] M. Ali, et al. J. Phys. Chem. C 117 (2013) 18234.
[55] M. Ali, et al. ACS Nano 4 (2010) 7267.
[56] M. Ali, et al. J. Am. Chem. Soc. 133 (2011) 17307.
[57] D.A. Doyle, et al. Science 280 (1998) 69.
[58] S. Garaj, et al. Nature 467 (2010) 190.
[59] K. Sint, et al. J. Am. Chem. Soc. 130 (2008) 16448.
[60] X.J. Gong, et al. J. Am. Chem. Soc. 132 (2010) 1873.
[61] Z. He, et al. ACS Nano 7 (2013) 10148.
[62] A.N. Lopatin, et al. Nature 372 (1994) 366.
[63] Z. Siwy, A. Fuliński, Phys. Rev. Lett. 89 (2002) 198103/1.
[64] Z. Siwy, et al. Phys. Rev. Lett. 94 (2005).
[65] Z.S. Siwy, Adv. Funct. Mater. 16 (2006) 735.
[66] I. Vlassiouk, Z.S. Siwy, Nano Lett. 7 (2007) 552.
[67] H. Daiguji, et al. Nano Lett. 5 (2005) 2274.
[68] H. Zhang, et al. J. Am. Chem. Soc. 135 (2013) 16120.
[69] C. Rischel, et al. Phys. Rev. Lett. 91 (2003) 1798011.
[70] P. Reimann, Phys. Rep. 361 (2002) 57.
[71] P. Ramirez, et al. Electrochem. Commun. 31 (2013) 137.
[72] D. Khananshvili, Pflugers Arch., EJP 466 (2014) 43.
[73] X. Xie, et al. Nat. Chem. 6 (2014) 202.
[74] Y.X. Jiang, et al. Nature 423 (2003) 33.
[75] S. Hernández-Ainsa, et al. Nano Lett. (2014).
[76] C. Plesa, et al. ACS Nano 8 (2013) 35.
[77] C.C. Harrell, et al. J. Am. Chem. Soc. 126 (2004) 15646.
[78] M. Muthukumar, Polymer Translocation, Taylor and Francis, 2011.
[79] M. Tsutsui, et al. ACS Nano 6 (2012) 3499.
[80] M. Tagliazucchi, et al. Proc. Natl. Acad. Sci. U.S.A. 110 (2013) 3363.
[81] S.W. Kowalczyk, et al. Nat. Nanotechnol. 6 (2011) 433.
[82] T. Jovanovic-Talisman, et al. Nature 457 (2009) 1023.
[83] S.M. Iqbal, et al. Nat. Nanotechnol. 2 (2007) 243.
[84] E.C. Yusko, et al. Nat. Nanotechnol. 6 (2011) 253.
[85] H. Huang, et al. Nat. Commun. 4 (2013).

Please cite this article in press as: M. Tagliazucchi, I. Szleifer, Mater. Today (2014), http://dx.doi.org/10.1016/j.mattod.2014.10.020